

# NUTRIENT UPTAKE BY A SELF-PROPELLED STEADY SQUIRMER

by VANESA MAGAR<sup>†</sup>

(*Department of Applied Mathematics and Theoretical Physics, University of Cambridge,  
Silver Street, Cambridge CB3 9EW*)

TOMONOBU GOTO

(*Department of Mechanical Engineering, Tottori University, Koyama, Tottori 680-8552,  
Japan*)

and T. J. PEDLEY

(*Department of Applied Mathematics and Theoretical Physics, University of Cambridge,  
Silver Street, Cambridge CB3 9EW*)

[Received 27 February 2001. Revises 25 January and 29 April 2002]

## Summary

In this paper we study nutrient uptake by a very simple model of a swimming microorganism, a sphere moving its surface tangentially to itself with constant concentration on the surface. The effect of its swimming motions on the concentration field and uptake is investigated. We find the relationship between the Sherwood number ( $Sh$ ), a measure of the mass transfer across the surface, and the Péclet number ( $Pe$ ), which indicates the relative effect of convection versus diffusion. Then we compare the results with those for a rigid sphere moving at the same speed under the action of an external force.

Analytical and computational results prove that there is little difference between the two cases when the flow field is dominated by diffusion, but substantial differences arise when convection plays an important role. In particular, for  $Pe$  large enough,  $Sh$  for a steady squirmer increases as the square root of  $Pe$ , compared with the cube root for a rigid sphere. For intermediate values of  $Pe$ , only numerical results are available, and they are obtained using a Legendre polynomial method and a separate finite volume method, allowing us to compare the two sets of results and assess the procedures used to obtain them. In Appendix A we discuss the effect of an alternative boundary condition on the Sherwood number expansions at small and large  $Pe$ .

## 1. Introduction

Computer models of populations of microscopic marine organisms are widely used in the study of phenomena such as harmful algal blooms, or the impact of nutrients on planktonic ecosystems (1). The rate of nutrient uptake by phytoplankton (plant-like microorganisms living in the upper layers of the ocean) constitutes an important element of such models. The amount of nutrient absorbed determines how large a microorganism can grow, and whether it can reproduce. When food is depleted from the water, the microorganisms either die or become cysts and wait again

---

<sup>†</sup> (V.Magar@damtp.cam.ac.uk)

for appropriate nutrient conditions. Therefore, studying the mass transfer to microorganisms is important for plankton ecology. In particular, little is known about how their swimming motion might affect the nutrient uptake rate: swimming could modify the concentration field near the surface by stirring the concentration boundary layer and bringing more nutrient-rich fluid near to the cell surface, thereby increasing the uptake.

In this paper we investigate the effect of swimming on nutrient absorption in the simplest model problem we can think of. The model microorganism is a sphere which moves its surface steadily and tangentially to itself. This is called a spherical *steady squirmer*; a model of a nearly spherical squirming organism was introduced by Lighthill (2), and the velocity field calculations were completed by Blake (3). In this paper we consider the radial velocity at the surface to be zero, and the tangential velocity to be independent of time; we also assume this time independence for the mass concentration in the ambient fluid.

Some microorganisms, like *Opalina* for example, move through the water by the beating of many little hairs (called *cilia*) attached to the surface. The cilia can follow different types of synchronized movement: when they remain densely packed throughout the motion, the time-dependent, wave-like squirming of the envelope covering the ends of the cilia can model the motion. Some authors (4, 5) have argued that this same envelope model could be applied directly to tiny blue-green algae, also called cyanobacteria, if one assumes that they propel themselves through the water by surface distortions. In fact, Ehlers *et al.* (5) used this assumption to find an approximation for the swimming speed of a microorganism propelling itself by means of small-amplitude, high-frequency sinusoidal waves travelling along the outer cell membrane. Skerker and Berg (6) have recently made direct observations of extension and contraction of some elements localized on the surface of certain cyanobacteria, but only at the tail of the microorganism. These protrusions are believed to be responsible for imparting the necessary swimming thrust. However, in order to show qualitatively that swimming motions can dramatically affect nutrient uptake, we will consider the model for self-propulsion used by Lighthill (2), and we will model the microorganism as a spherical squirmer, that is, we do not investigate any shape effects or unsteady effects. All these simplifications and modelling assumptions mean that we cannot claim realism for our simple model. Unsteady spherical squirmers will be considered in a subsequent paper, and we will modify our model still further in future work so that the results become realistic.

Our objective is to determine the Sherwood number  $Sh$ , a measure of the rate of mass transfer, as a function of the Péclet number  $Pe$ , which indicates the importance of convection relative to diffusion, and compare it with that of a rigid sphere moving at the same speed under the action of an external force. In the microscopic realm, the range of values the Péclet number can take is large. For instance, for a bacterium and a cyanobacterium  $Pe$  is  $O(10^{-3})$  to  $O(10^{-2})$ , but for a ciliate such as *Opalina*  $Pe$  may be of order  $10^2$ . Thus, it is important to see whether swimming is important for any value of the Péclet number. We use the known velocity field in the convection–diffusion equation to find the mass concentration, and thereby determine the functional relationship between  $Sh$  and  $Pe$ , both analytically for small and large Péclet numbers, and numerically for the whole range of values.

For small  $Pe$ , the procedure followed is the same as that presented by Acrivos and Taylor (7) for heat transfer from a rigid sphere. For large  $Pe$ , the asymptotic behaviour can be deduced from boundary-layer theory. Finally, we obtain numerical results for all values of  $Pe$ . All the calculations are made under the assumption that the nutrient concentration is constant and uniform at the cell surface. A different boundary condition, possibly more applicable to nutrient absorption by living cells, is explored in Appendix A. We check the accuracy of the numerical results by comparing

with the asymptotic behaviours, pointing out some discrepancies between numerical and analytical results for large  $Pe$ . We also see the extent to which the swimming motions enhance mass transfer by comparing with the results for a rigid sphere.

## 2. The flow field

We consider the scaling  $\mathbf{U} = \mathbf{U}^*/U^*$ , where  $U^*$ , the characteristic velocity, is the velocity of translation of the squirmer in still fluid and in the absence of a body force;  $\mathbf{U}^*$  is the velocity field, and an asterisk indicates a dimensional variable. As stated above, the radial velocity at the surface is zero. The Reynolds number  $Re$  for the microorganisms we are interested in studying is in the range  $10^{-5}$  (for a bacterium) to  $10^{-1}$  (for a ciliate protozoon) (8), which allows us to use the Stokes equations for the flow field.

All the analysis is in a frame such that the squirmer has zero translational velocity, and there is a uniform flow of speed  $U^*$  coming from the far right (see Fig. 1). The velocity field for  $r^* > a$ , relative to axes fixed in the sphere, is obtained by solving the differential equation for the Stokes stream function, and by applying the appropriate boundary conditions both at the surface and at infinity, together with the condition of axial symmetry. For the steady squirmer, the velocity components are (3)

$$U_r^* = -U^* \mu + \frac{2B_1 a^3}{3r^{*3}} P_1(\mu) + \sum_{n=2}^{\infty} \left( \frac{a^{n+2}}{r^{*n+2}} - \frac{a^n}{r^{*n}} \right) B_n P_n(\mu)$$

and

$$U_\mu^* = U^* (1 - \mu^2)^{\frac{1}{2}} + \frac{B_1 a^3}{3r^{*3}} V_1(\mu) + \sum_{n=2}^{\infty} \left[ \frac{na^{n+2}}{2r^{*n+2}} - \left( \frac{n}{2} - 1 \right) \frac{a^n}{r^{*n}} \right] B_n V_n(\mu),$$

where  $r^*$  is the distance from the centre in spherical polar coordinates,  $\mu = \cos \theta$ ,  $P_n$  is the Legendre polynomial of order  $n$ , and we define

$$V_n = \frac{2}{n(n+1)} (1 - \mu^2)^{\frac{1}{2}} P_n'(\mu) = -\frac{2}{n(n+1)} P_n^1(\mu).$$

For the motion to have finite total energy it is necessary that  $U^* = 2B_1/3$  (3). Also, we assume the characteristic lengthscale to be the radius  $a$  of the sphere (as shown in Fig. 1), so that the dimensionless radial coordinate is  $r = r^*/a$ . Then the velocity field in non-dimensional form is given by

$$U_r = -\mu + \frac{1}{r^3} P_1(\mu) + \frac{3}{2B_1} \sum_{n=2}^{\infty} \left( \frac{1}{r^{n+2}} - \frac{1}{r^n} \right) B_n P_n(\mu) \quad (2.1)$$

and

$$U_\mu = (1 - \mu^2)^{\frac{1}{2}} + \frac{1}{2r^3} V_1(\mu) + \frac{3}{2B_1} \sum_{n=2}^{\infty} \left[ \frac{n}{2r^{n+2}} - \left( \frac{n}{2} - 1 \right) \frac{1}{r^n} \right] B_n V_n(\mu). \quad (2.2)$$

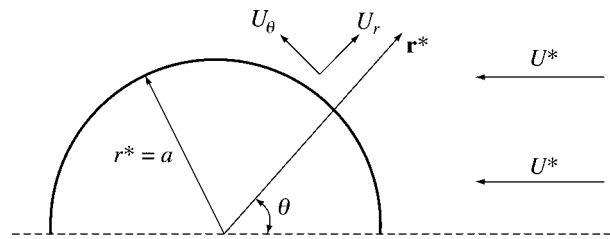


**Fig. 1** The model microorganism. The spherical self-propelled body is moving with uniform velocity  $U^*$ . The tangential velocity at the surface is non-zero

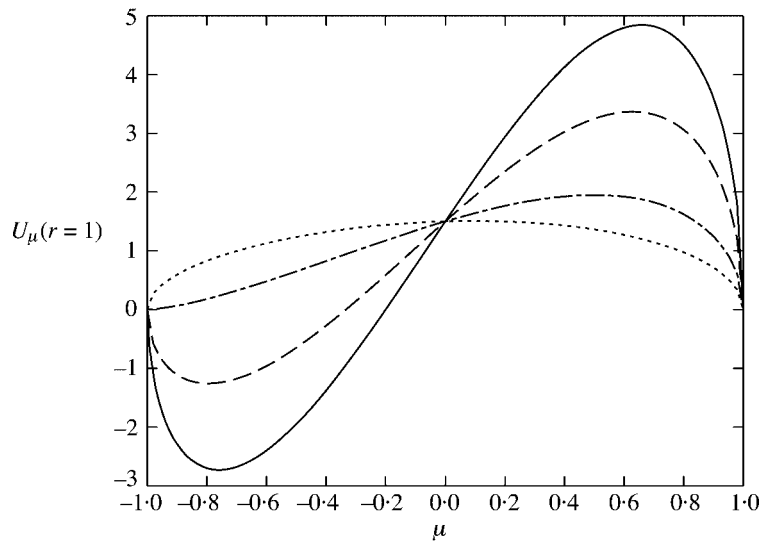


**Fig. 2** Tangential velocity at the surface of the squirmer for (a)  $q = 5$  (solid line); (b)  $q = 3$  (dashed line); (c)  $q = 1$  (dashed and dotted line); and (d)  $q = 0.1$  (dotted line)

While the radial velocity vanishes (by definition of a squirmer), the tangential velocity at the surface is a function of the polar angle  $\theta$ . For the purpose of detailed calculation, we take  $B_n = 0$  for  $n > 2$ , and  $U$  and  $B_2$  are constants. This is a large simplification since we need several harmonics and time-dependent functions to describe a realistic wave propagating over the surface. However, these two coefficients are sufficient to illustrate the effects being investigated. In Fig. 2 we plot  $U_\mu$  at the surface for a few positive values of the parameter  $q$ , which is defined as  $q = B_2/B_1$ . When  $q$  is negative, the plots are symmetrical to the  $\mu = 0$  axis. Now, we know that the characteristic velocity is proportional to  $B_1$ , and Fig. 2 shows that  $U_\mu$  vanishes at a third point of the surface of the microorganism when  $|q| > 1$ . Therefore, when  $|q| > 1$  we expect a recirculation region to appear

at the back of the microorganism, which means that  $q$  represents a measure of the stirring of the water due to the movement of the surface versus the translation of the self-propelled body.

### 3. The mass transfer equation

The convection–diffusion equation satisfied by the nutrient concentration  $C^*$  is given by

$$C_{t^*}^* + \mathbf{U}^* \cdot \nabla^* C^* = D \nabla^{*2} C^*, \quad (3.1)$$

where  $D$  is the diffusivity of nutrients. If the concentration of nutrients is uniform at the surface, with the value  $C_0^*$ , and at infinity  $C_\infty^*$ , then we can consider the classical scaling

$$C = \frac{C_\infty^* - C^*}{C_\infty^* - C_0^*},$$

so that the boundary conditions are  $C = 1$  at the surface and  $C \rightarrow 0$  as  $r$  tends to infinity. As we said before, in Appendix A we explore how the results are affected if we take an alternative condition on the concentration at the boundary which seems more realistic. In the steady case the non-dimensional form of (3.1) is

$$\text{Pe} (\mathbf{U} \cdot \nabla C) = \nabla^2 C, \quad (3.2)$$

where  $\text{Pe} = aU/D$ , the Péclet number, is based on the radius of the squirmer, and  $\mathbf{U}$  is given by (2.1) and (2.2). Since the diffusivity  $D$  of all solutes is small compared to the kinematic viscosity  $\nu$  of water,  $\text{Pe}$  can be large. The non-dimensional uptake rate, the Sherwood number, is given by

$$\text{Sh} = - \int_{-1}^1 \left( \frac{\partial C}{\partial r} \right)_{r=1} d\mu. \quad (3.3)$$

Our goal is to find  $\text{Sh}$  as a function of  $\text{Pe}$ . We will start by considering small values of the parameter  $\text{Pe}$ .

### 4. Analytical solution for small Péclet numbers

Following Acrivos and Taylor (7) we solve the problem in the limit of small  $\text{Pe}$  using the method of matched asymptotic expansions. In the inner region,  $r = O(1)$  and the governing equation is (3.2); in the outer region, we use the radial variable  $\rho = (\text{Pe}) r$ , and the governing equation ceases to contain  $\text{Pe}$  explicitly. We let  $C_{\text{in}}$  and  $C_{\text{out}}$  represent the expansions for  $C$  in the two regions respectively. The two expansions must be equivalent in an intermediate region. For the current problem, the inner solution is regular up to  $O(\text{Pe}^2)$ , and the final result is

$$C_{\text{in}} = (C_{\text{in}})_0 + \text{Pe} (C_{\text{in}})_1 + \text{Pe}^2 (C_{\text{in}})_2 + \dots,$$

with

$$\begin{aligned} (C_{\text{in}})_0 &= \frac{1}{r}, \\ (C_{\text{in}})_1 &= -\frac{1}{2} \left( 1 - \frac{1}{r} \right) + \left( -\frac{1}{2} - \frac{1}{4r^3} + \frac{3}{4r^2} \right) \mu \\ &\quad - \frac{3q}{2} \left( \frac{1}{6r^4} + \frac{1}{4r^2} - \frac{5}{12r^3} \right) P_2(\mu) \end{aligned}$$

and

$$\begin{aligned} (C_{\text{in}})_2 = & -\frac{1}{4} \left(1 - \frac{1}{r}\right) + R_0(r) - R_0(1)r^{-1} \\ & + \mu \left[ \frac{1}{4} \left(r - \frac{1}{r^2}\right) + R_1(r) - R_1(1)r^{-2} \right] \\ & + \sum_{n=2}^4 \left[ R_n(r) - R_n(1)r^{-(n+1)} \right] P_n(\mu), \end{aligned}$$

where  $R_0, \dots, R_4$  in  $(C_{\text{in}})_2$  are polynomials of  $r$ . The Sherwood number defined in (3.3) can be computed from the inner solution alone. Also, in order to determine the coefficient of the  $O(\text{Pe}^2)$  term of the Sherwood number expansion, we only need  $R_0(r)$ , which is of the form

$$\begin{aligned} R_0(r) = & \frac{r}{6} + \frac{1}{24r^2} - \left(\frac{3q^2}{80}\right) \frac{1}{r^3} + \left(\frac{3q^2}{64} - \frac{1}{16}\right) \frac{1}{r^4} \\ & + \left(\frac{1}{60} + \frac{3q^2}{400}\right) \frac{1}{r^5} - \left(\frac{q^2}{32}\right) \frac{1}{r^6} + \left(\frac{3q^2}{280}\right) \frac{1}{r^7}. \end{aligned}$$

The explicit forms of the functions  $R_1, \dots, R_4$  are given in Appendix B. From the above, the Sherwood number can be shown to be given by

$$\text{Sh} = 2 + \text{Pe} + \left(-\frac{13}{40} + \frac{41q^2}{5600}\right) \text{Pe}^2. \quad (4.1)$$

It is worth remarking that the corresponding expansion for the rigid sphere includes a term of order  $\text{Pe}^2 \ln(\text{Pe})$  (7). This is absent in our case as a result of the fact that for a self-propelled body there is no external force, so that the velocity field decays as  $1/r^2$  as  $r \rightarrow \infty$ , not  $1/r$  as for the rigid sphere. However, the first two terms are the same in the two cases, reflecting the fact that the differences are not very important when the mass transfer is diffusion-dominated.

### 5. Asymptotic solution for large Péclet number

When  $\text{Pe}$  takes large values, a concentration boundary layer is expected to form near the surface of the microorganism, in the region where  $r - 1 \ll 1$ . The thickness of this boundary layer can be estimated by introducing the variable

$$Y = \text{Pe}^m (r - 1).$$

The velocity is  $O(1)$  near the surface, and it follows from the mass transfer equation that  $m = \frac{1}{2}$ , that is, the boundary-layer thickness is  $O(\text{Pe}^{-\frac{1}{2}})$ . In the rigid sphere case  $m = \frac{1}{3}$ —the boundary-layer thickness being  $O(\text{Pe}^{-\frac{1}{3}})$ —because the velocity field near the surface is  $O(r - 1)$ . Thus there is a marked difference between the two cases. In fact, the mass transfer is enhanced by squirming, since the Sherwood number is proportional to  $\text{Pe}^{\frac{1}{2}}$ , not  $\text{Pe}^{\frac{1}{3}}$ , with constant of proportionality  $c$ , say

$$\text{Sh} = c\text{Pe}^{\frac{1}{2}}. \quad (5.1)$$

In order to determine  $c$ , we need to find a similarity variable  $\eta$  so that  $C$ , in the mass transfer equation

$$\frac{\partial^2 C}{\partial Y^2} = -3Y \left[ \mu + \frac{q}{2} (3\mu^2 - 1) \right] \frac{\partial C}{\partial Y} - \frac{3}{2} (1 - \mu^2) (1 + q\mu) \frac{\partial C}{\partial \mu}, \tag{5.2}$$

depends only on  $\eta$ . Equation (5.2) is the *concentration boundary-layer equation* for this problem (9), and when a similarity solution  $C(\eta)$  exists, this equation can be transformed into an ordinary differential equation for  $C$ , with coefficients which are either a constant or a function of  $\eta$ . It is customary in heat transport processes at large Péclet numbers to seek  $\eta$  in the form  $\eta = Y/g(\mu)$ , for some positive function  $g(\mu)$ . Here  $Y$  is the concentration boundary-layer coordinate normal to the body surface at each point, and  $g(\mu)$  represents the  $\mu$ -dependence of the boundary-layer thickness. Now, if we substitute  $\eta$  and the derivatives of  $C$  with respect to  $\eta$  required in equation (5.2), we obtain

$$\frac{\partial^2 C}{\partial \eta^2} - \left\{ \frac{3}{4} (1 - \mu^2) (1 + q\mu) (g^2)' - 3 \left[ \mu + \frac{q}{2} (3\mu^2 - 1) \right] g^2 \right\} \frac{\partial C}{\partial \eta} = 0. \tag{5.3}$$

Then, a necessary condition for a similarity solution to exist is that

$$\frac{3}{4} (1 - \mu^2) (1 + q\mu) (g^2)' - 3 \left[ \mu + \frac{q}{2} (3\mu^2 - 1) \right] g^2 = \text{constant}. \tag{5.4}$$

However, this condition is not sufficient for we also need to find a solution of equation (5.3) which is compatible with the boundary conditions imposed on  $C$ . If, without loss of generality, we take the constant as  $-2$ , equations (5.4) and (5.3) can easily be solved. In fact, the expression for  $C$  is given by

$$C = \text{erfc}(\eta), \tag{5.5}$$

whereas that for  $g$  is of the form

$$g = 2\sqrt{2/3} \frac{(k - \mu - q\mu^2/2 + \mu^3/3 + q\mu^4/4)^{1/2}}{(1 - \mu^2)(1 + q\mu)}. \tag{5.6}$$

From equation (5.6) we deduce that  $g$  may be singular at the front and rear stagnation points, that is, at  $\mu = 1$  and  $\mu = -1$ , respectively. It may be singular at  $\mu = -1/q$  also but only when  $|q| > 1$ . In the next two subsections, we explain how to choose  $k$  on physical considerations, so that  $g$  is bounded at the appropriate points: we will allow  $g$  to be singular at points where we expect the boundary-layer scaling to break down (for example, near the wake), but we will adjust  $k$  so that  $g$  is bounded otherwise.

### 5.1 $q > -1$

The point at which we will choose  $g$  to be bounded will be a stagnation point at which the flow impinges on the sphere surface. In the case when  $q > -1$  that point corresponds to the front stagnation point  $\mu = 1$ , and we set the constant  $k$  as  $\frac{2}{3} + \frac{1}{4}q$  so that  $g$  is bounded there.

From (3.3), the constant of proportionality is given by

$$c = \frac{2}{\sqrt{\pi}} \int_{\alpha}^1 \frac{d\mu}{g(\mu)}, \tag{5.7}$$

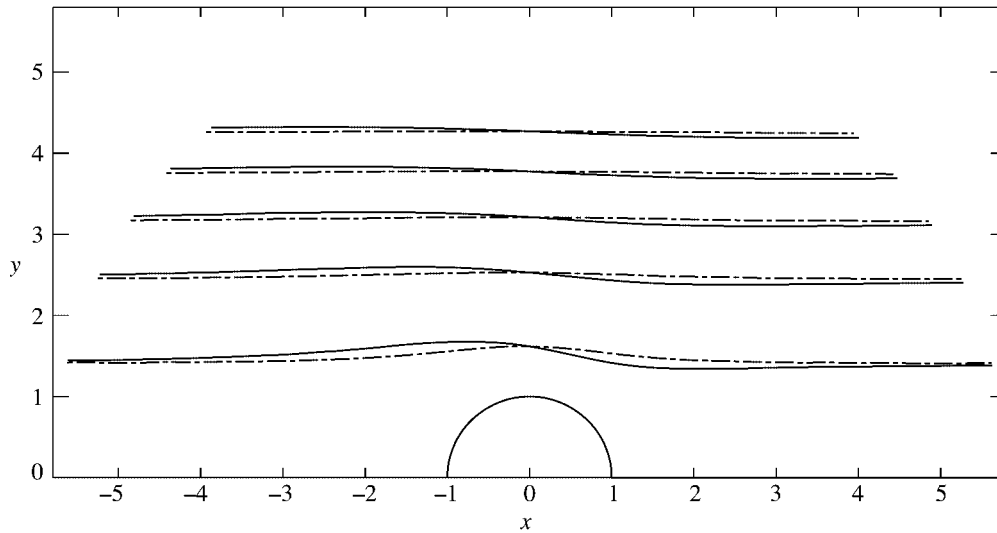


**Fig. 3** Stream function contours when  $|q| \leq 1$ . The solid line corresponds to  $q = 0.1$ , and the dash-dotted one to  $q = 1$ . The flow comes from the right and is unidirectional, so that there are no closed streamlines in any region. The stream function contours correspond to values of the stream function from  $-1$  to  $-9$  in steps of 2, and to the value 0

where the lower limit  $\alpha$  is equal to  $-1$  if we can apply the above boundary-layer theory over the whole surface, that is, when  $q < 1$ . However, when  $q > 1$  the tangential velocity on the surface vanishes at  $\mu = -1/q$ , as we know from Fig. 2, and a recirculation region appears at the back of the squirmer. Flow streamlines for various values of  $q$  are plotted in Figs 3 and 4, and they show that the recirculation region becomes larger as  $q$  increases. Only the front part of the sphere is exposed to streamlines that originate upstream at infinity, bringing fresh nutrient close to the surface.

Mass transfer is likely to be significantly reduced at the rear, so in this case we take  $\alpha = -1/q$ . Comparison with the numerical solution will provide a test for this assumption. From (5.7) we thus obtain

$$c = c_- = \sqrt{\frac{8}{\pi}} \quad \text{when } |q| \leq 1, \quad (5.8)$$

$$c = c_+ = \sqrt{\frac{6}{\pi}} \left( \frac{2}{3} + \frac{q}{4} + \frac{1}{2q} - \frac{1}{12q^3} \right)^{\frac{1}{2}} \quad \text{when } q > 1. \quad (5.9)$$

Formula (5.9) is valid for all  $q$  larger than 1, because in that range the function under the square root sign is always positive;  $q$  positive means that squirming is in the same direction as the uniform flow. We also remark that  $c$  is constant when  $|q| \leq 1$ —because then the terms depending on  $q$  in the expression for  $c$  cancel each other—and that  $c$  increases as  $q$  increases when  $q > 1$ . Therefore, when  $q > 1$ , the larger  $q$ , the greater the mass transfer, for a given swimming speed.

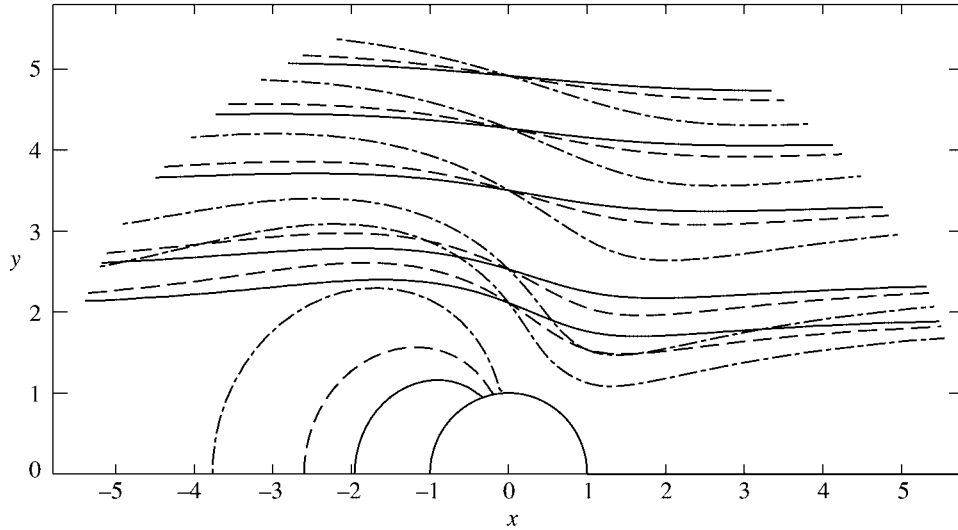


**Fig. 4** When  $|q| > 1$ , the tangential velocity on the surface vanishes at an angle  $\theta_0 = \cos^{-1}(-1/q)$ . So for  $\theta_0 < \theta < \pi$ , there is a recirculation region at the back of the microorganism, in which boundary-layer theory cannot be applied. Here stream function contours are plotted for  $q = 3$  (solid),  $q = 5$  (dashed) and  $q = 10$  (dash-dotted). The contours are symmetrical with respect to the  $y$ -axis for negative  $q$ , but the direction of the flow is still from right to left

### 5.2 $q < -1$

In the case when  $q < -1$ , boundary-layer theory may be applicable for  $-1 < \mu < -1/q$ . On physical grounds we expect the boundary layer to be thinnest at  $\mu = -1/q$  because the flow comes from the far right. We choose  $k$  in (5.6) so that  $g$  is bounded at  $\mu = -1/q$ , so we require that  $k = -1/2q + 1/12q^3$ . Then  $g$  may be written as

$$g = \frac{2\sqrt{2}}{\sqrt{3}} \frac{1}{(1-\mu^2)} \left( \frac{3q^2\mu^2 - 2q\mu + 1 - 6q^2}{12q^3} \right)^{\frac{1}{2}},$$

but only if the polynomial  $3q^2\mu^2 - 2q\mu + 1 - 6q^2$  is negative for all the values of  $\mu$ , because in that case the function under the square root is positive. Now, that polynomial is negative when  $\mu$  is in the interval  $\left[ \frac{1 + \sqrt{18q^2 - 2}}{3q}, \frac{1 - \sqrt{18q^2 - 2}}{3q} \right]$ . But when  $q < -1$ ,  $\frac{1 + \sqrt{18q^2 - 2}}{3q}$  is less than  $-1$ , and  $-1/q$  is less than  $\frac{1 - \sqrt{18q^2 - 2}}{3q}$ . Therefore, the polynomial is negative when  $\mu$  is in the range of values for which boundary-layer theory is applicable, that is, between  $-1$  and  $-1/q$ , and we can define  $g$  as above.

From (3.3), we determine the constant of proportionality  $c$  with the integral

$$c = \frac{2}{\sqrt{\pi}} \int_{-1}^{-1/q} \frac{d\mu}{g(\mu)}, \quad (5.10)$$

which can be readily found to be

$$c = c_- = \sqrt{\frac{6}{\pi}} \left( -\frac{q}{4} + \frac{2}{3} - \frac{1}{2q} + \frac{1}{12q^3} \right)^{\frac{1}{2}}. \quad (5.11)$$

The equation above shows that  $c$  decreases as  $|q|$  decreases for all  $q < -1$ , up to the value of  $c_- = 1.6$  when  $q = -1$ . Therefore, the greater  $|q|$ , the greater the mass transfer to the steady squirmer. Moreover, it is easy to deduce from (5.9) and (5.11) that  $c_-(-q) = c_+(q)$ , which, together with (4.1), lead us to the conclusion that  $\text{Sh}(q) = \text{Sh}(-q)$  both at small and large Péclet numbers, despite the fact that the flow is not reversible. This non-intuitive result helps to validate our analysis, because it is consistent with a theorem, proved by Brenner (10), that the net rate of heat flow from a particle into an incompressible Stokes flow is independent of direction.

Finally, it is worth noting that if  $k = -\frac{2}{3} + \frac{1}{4}q$ ,  $g$  is bounded at  $\mu = -1$ , the other stagnation point, but then the function under the square root is negative for all  $\mu$  if  $q < -\frac{1}{3}$ , in particular, if  $q < -1$ . Another argument is to see that when  $q$  is less than  $-1$ ,  $-1/q$  is positive and then  $\mu = 0$  is in the range of integration for  $c$ . However, when  $\mu$  is zero  $g$  is proportional to  $k^{\frac{1}{2}}$ , and therefore it is necessary that  $k > 0$ , or  $q > \frac{8}{3}$ , which is a contradiction.

## 6. Numerical methods

### 6.1 The Legendre polynomial expansion method (LPEM)

It is quite difficult to achieve good accuracy in the numerical solution of equation (3.2), at larger values of  $\text{Pe}$ . Therefore we have used two different methods, as a test of each other. In the first, we follow the analysis of Dennis *et al.* (11) for the heat transfer to a rigid sphere. We write the concentration  $C$  as a Legendre polynomial expansion, so that

$$C = \sum_{n=0}^{\infty} C_n(\xi) P_n(\mu), \quad (6.1)$$

where  $\xi = \ln(r)$ ; we take this radial variable so that mesh points near the surface of the squirmer are more densely packed. Then we need to solve only a system of ordinary differential equations for  $C_n(\xi)$ . In spherical polar coordinates, equation (3.2) is

$$\left[ \frac{1}{r^2} \frac{\partial}{\partial r} \left( r^2 \frac{\partial}{\partial r} \right) + \frac{1}{r^2} \frac{\partial}{\partial \mu} \left\{ (1 - \mu^2) \frac{\partial}{\partial \mu} \right\} \right] C = \epsilon \left[ U_r \frac{\partial C}{\partial r} - \frac{(1 - \mu^2)^{\frac{1}{2}}}{r} U_\mu \frac{\partial C}{\partial \mu} \right], \quad (6.2)$$

where  $\epsilon = \text{Pe}$ . If we substitute the velocity field (2.1), (2.2), introduce the Legendre series expansion, and multiply both sides by  $\exp(2\xi)$ , the left-hand side (LHS) becomes

$$\text{LHS} = \sum_{n=0}^{\infty} [C_n'' + C_n' - n(n+1)C_n] P_n(\mu),$$

whereas the right-hand side (RHS) takes the form

$$\begin{aligned} \text{RHS} = & \epsilon \left[ \exp(-2\xi) - \exp(\xi) \right] \sum_{n=0}^{\infty} \sum_{k=0}^{\infty} \alpha_1(n, k) C'_k(\xi) P_n(\mu) \\ & + \epsilon \frac{3q}{2} \left[ \exp(-3\xi) - \exp(-\xi) \right] \sum_{n=0}^{\infty} \sum_{k=0}^{\infty} \alpha_2(n, k) C'_k(\xi) P_n(\mu) \\ & - \frac{2}{3} \epsilon \left[ \exp(\xi) + \frac{1}{2} \exp(-2\xi) \right] \sum_{n=0}^{\infty} \sum_{k=0}^{\infty} \beta_{0,2}(n, k) C_k(\xi) P_n(\mu) \\ & - \frac{3q}{5} \epsilon \exp(-3\xi) \sum_{n=0}^{\infty} \sum_{k=0}^{\infty} \beta_{1,3}(n, k) C_k(\xi) P_n(\mu), \end{aligned}$$

where

$$\alpha_i(n, k) = \frac{2n+1}{2} \int_{-1}^1 P_i P_k P_n dt$$

and

$$\beta_{i,j}(n, k) = \frac{2n+1}{2} \int_{-1}^1 [P_i - P_j] P'_k P_n dt.$$

The boundary conditions to be satisfied are  $C_0 = 1$  and  $C_n = 0$ , for  $n > 0$ , at the surface. If we choose a suitably large value  $\xi_{\max}$ , which will depend on the range of Pe considered, we can approximate at that value the boundary condition at infinity, so we take  $C_n = 0$  for all  $n$ , at  $\xi = \xi_{\max}$ . Another way of approximating that boundary condition is described by Dennis *et al.* (11), who proved that as  $r \rightarrow \infty$  the concentration is exponentially small except in a wake region for which  $\pi - \theta = O(r^{-\frac{1}{2}})$ . These same authors then proved that the boundary condition at a large boundary mesh point  $i = M$  can be related to the previous mesh point  $i = M - 1$  through the condition

$$C_n(Mh + h) = \exp(-2h) C_n(Mh). \tag{6.3}$$

This is due to the fact that, at large  $\xi$ , the functions  $C_n(\xi)$  are asymptotically equal to  $D_n \exp(-2\xi)$ . In section 7.3 we will compare some results obtained using equation (6.3) or  $C_n(Mh) = 0$  as the conditions at the outer boundary, but in general we consider  $C_n(Mh) = 0$  because, as we will see, the difference between results is very small. Moreover, since it is impossible to consider an infinite number of functions  $C_n$ , we truncate the series (6.1) after  $N$  terms, and increase  $N$  until the predicted value of Sh ceases to change significantly.

The quantities  $\alpha_i$  and  $\beta_{i,j}$  can be found explicitly by using the recurrence relations for Legendre polynomials. Their values are given in Appendix C. Thus the mass transfer equation can be written as

$$\begin{aligned} C_n'' + f_{pi} C_n' + f_i C_n + f_{pj} C_{n+1}' + f_j C_{n+1} + f_{pk} C_{n+2}' \\ + f_k C_{n+2} + f_{ph} C_{n-1}' + f_h C_{n-1} + f_{pg} C_{n-2}' + f_g C_{n-2} = 0, \end{aligned}$$

where the functions in the expression above depend on  $n$ ,  $\xi$  and  $q$ . Then we introduce three-point finite differences to discretize the equation, and together with the boundary conditions, we need finally to solve a system of the form

$$\underline{\underline{\mathbf{M}}} \mathbf{X} = \mathbf{B}, \quad (6.4)$$

where the resultant matrix  $\underline{\underline{\mathbf{M}}}$  is block quindagonal, in which each of the blocks is a tridiagonal matrix. This can be solved quite easily by using block Gaussian elimination. In our problem the matrix  $\underline{\underline{\mathbf{M}}}$  is too ill-conditioned for an iterative method to work well, so a direct method was selected. Finally, the Sherwood number was determined by using the interpolatory [r,s] method, described by Iserles (12). This method states that the first derivative at the origin can be written as a series of the values at the grid points of the function itself, so that

$$\left[ \frac{\partial C_0}{\partial \xi} \right]_{\xi=0} = \frac{1}{h} \sum_{i=0}^s \alpha_i C_0(ih),$$

where  $h$  is the grid size. The  $\alpha_i$  are of the form

$$\alpha_0 = \sum_{j=1}^s \frac{1}{j} \quad \text{and} \quad \alpha_i = \frac{(-1)^{i+1}}{i} \frac{s!}{i!(s-i)!}.$$

We choose  $s = 5$ , because the rigid sphere results for larger values of  $s$  are not accurate when compared to the ones obtained by Acrivos and Taylor (7), for small Péclet number. Then, the formula to calculate the Sherwood number is

$$\text{Sh} = -2 \left( \frac{1}{h} \right) \left[ -\frac{137}{60} + 5 C_0(h) - 5 C_0(2h) + \frac{10}{3} C_0(3h) - \frac{5}{4} C_0(4h) + \frac{1}{5} C_0(5h) \right]. \quad (6.5)$$

## 6.2 The finite volume method (FVM)

The second numerical procedure is based on a type of finite volume discretization. Equation (3.2) has the identical solution to the steady solution of the following time-dependent equation:

$$\int \frac{\partial C}{\partial t} dV + \int \mathbf{u} \cdot \mathbf{n} C dS - \frac{1}{\text{Pe}} \int \nabla C \cdot \mathbf{n} dS = 0, \quad (6.6)$$

which is in integral form. Time is non-dimensionalised by  $a/U$ , and the velocity field is divergence free. We solve equation (6.6) in an orthogonal coordinate system  $\boldsymbol{\xi} = (\xi, \eta)$ , whose components correspond to the  $r$  and  $\theta$  coordinates, respectively, instead of the  $\mathbf{x} = (x, y)$  coordinate system. The coordinate  $\xi$  is defined by a logarithmic function of  $r$ , and the form of this function depends on the radius of the outer boundary, on a parameter  $imax$ , and on the boundary-layer thickness. Then, equation (6.6) becomes

$$\int \frac{\partial C}{\partial t} dV + \int C \left( \left| \frac{\partial \mathbf{x}}{\partial \xi} \right| U, \left| \frac{\partial \mathbf{x}}{\partial \eta} \right| V \right) d\mathbf{S} - \frac{1}{\text{Pe}} \int \left( \left| \frac{\partial \mathbf{x}}{\partial \xi} \right|^{-1} \frac{\partial C}{\partial \xi}, \left| \frac{\partial \mathbf{x}}{\partial \eta} \right|^{-1} \frac{\partial C}{\partial \eta} \right) d\mathbf{S} = 0, \quad (6.7)$$

where  $S$  is the surface area in physical space and is normal to  $\xi$  or  $\eta$ , and  $\mathbf{U} = (U, V) = (\xi_x u + \xi_y v, \eta_x u + \eta_y v)$  is the contravariant velocity. Defining  $\bar{C}$  as the average value of  $C$  in a computational cell, we rewrite equation (6.7) as

$$\frac{\partial}{\partial t} \bar{C}_{i,j} V + \int_{S_{i,j}} E(\bar{C}) dS - \frac{1}{\text{Pe}} \int_{S_{i,j}} F(\bar{C}) dS = 0, \quad (6.8)$$

for a cell  $(i, j)$  of volume  $V$ . Here,  $i$  represents the cell number in the  $\xi$  direction, and  $j$  the cell number in the  $\eta$  direction. The interval between the cells is chosen as unity in the  $\xi$  coordinate system.

In the equation above the derivative with respect to time can come out of the integral, for the volume is independent of time. There are several choices one can make for the numerical fluxes,  $E$  and  $F$ , through the cell surface. We adopt the ones equivalent to the second-order central difference scheme in both the convection and the diffusion terms, that is,

$$E_{i+\frac{1}{2},j} = \frac{1}{2} \left( U_{i+\frac{1}{2},j} \right) (\bar{C}_{i+1,j} + \bar{C}_{i,j}) \left| \frac{\partial \mathbf{x}}{\partial \xi} \right|, \quad (6.9)$$

$$F_{i+\frac{1}{2},j} = (\bar{C}_{i+1,j} - \bar{C}_{i,j}) \left| \frac{\partial \mathbf{x}}{\partial \xi} \right|^{-1}. \quad (6.10)$$

Time marching in equation (6.8), which can be written as

$$\begin{aligned} \Delta \bar{C} + \frac{\Delta t}{V} \int E(\Delta \bar{C}) dS - \frac{1}{\text{Pe}} \frac{\Delta t}{V} \int F(\Delta \bar{C}) dS \\ = -\frac{\Delta t}{V} \int E(\bar{C}^k) dS + \frac{1}{\text{Pe}} \frac{\Delta t}{V} \int F(\bar{C}^k) dS, \end{aligned} \quad (6.11)$$

is dealt with implicitly, so that numerical instabilities caused by the convection term are suppressed. The superscript  $k$  in (6.11) refers to the present time step and

$$\Delta \bar{C} = \bar{C}^{k+1} - \bar{C}^k;$$

(6.11) is a set of algebraic equations for  $\Delta \bar{C}_{i,j}$ , whose solution at time  $k+1$  may be obtained directly through inversion of an  $(imax \times jmax)^2$  matrix. Instead, we use an approximate factorization, which transforms the differential operator expressed by the original matrix into the product of a  $\xi$ -dependent operator and an  $\eta$ -dependent one, and they are both linear in  $t$ . In each step, these matrices are tridiagonal if the fluxes in equations (6.9), (6.10) are employed, and then the tridiagonal matrix algorithm is used to solve the equations.

The boundary condition on the squirmer ( $r = 1$ ) is set as

$$\frac{1}{2} (\bar{C}_{0,j} + \bar{C}_{1,j}) = 1. \quad (6.12)$$

The cell  $(1, j)$  is at the boundary of the squirmer and the dummy cell  $(0, j)$  inside it. For the condition at infinity, we set

$$\bar{C}_{imax+1,j} = \bar{C}_{imax,j}, \quad (6.13)$$

so that we neglect the effect of the diffusion on the boundary and the concentration is transferred only by the flow. In the  $\eta$  direction, the boundary condition of axisymmetry is automatically satisfied

since we consider triangular cells when the cells touch the  $z$ -axis, and therefore the area of the surface on the axis is zero.

The Sherwood number is calculated from

$$\text{Sh} = \frac{1}{2\pi} \sum_{j=1}^{jmax} F_{\frac{1}{2},j}. \quad (6.14)$$

The integral over the surface is replaced by the summation in this equation. The error caused by this simplification is estimated to be 0.004 per cent by the difference in surface area between the one given by this computation and the ideal one ( $4\pi a^2$ ). The computations are started impulsively:

$$\bar{C}_{0,j} = 2, \quad \bar{C}_{i,j} = 0 \quad (i \neq 0) \quad \text{at } t = 0. \quad (6.15)$$

Here  $\Delta t$  is 0.01, and the mesh numbers are fixed to  $imax = 1000$ ,  $jmax = 180$ . The meshes are clustered near the squirmer in the  $\xi$  direction; the smallest cell size in physical space is chosen as  $1.0 \times 10^{-2}$  for small  $Pe < 1$ , and  $1.0 \times 10^{-3}$  for large  $Pe$ , reflecting the thickness of the concentration boundary layer. In the  $\eta$  direction, the interval is  $1^\circ$ .

For small  $Pe$ , the computational domain extends to  $r = 5000$  (very large) in order to minimize the effect of taking the boundary condition at infinity at a finite value. The calculation is stopped at  $t = 100$ , which is before the effect of convection and diffusion reaches the boundary. For large Péclet number, the outer boundary is set at  $r = 50$ . When the sum of relative error in  $\bar{C}$  ( $\Delta\bar{C}/(\bar{C}\Delta t)$ ) over the computational domain becomes smaller than  $10^{-10}$ , we consider the solution to be steady. For large  $Pe$ , the calculation is stopped at that moment. The relative error in  $\text{Sh}$  per unit time is  $10^{-3}$  per cent at most.

## 7. Results and discussion

### 7.1 $q > -1$

**7.1.1 Small Péclet numbers.** For small  $Pe$ , convergence of the numerical results was attained for  $N = 5$ ,  $\xi_{\max} = 9$ , and  $h = 2 \times 10^{-2}$  for the LPEM. In preliminary calculations for a rigid sphere, we found that the LPEM is more accurate than the FVM for this range of Péclet numbers.

The results are shown in Fig. 5, for various values of the squirming parameter  $q$ . The difference between the results for  $q = 0.1$  and  $q = 1$  is not noticeable at this scale, but as soon as  $q$  becomes larger than 0.5, the Sherwood number increases as  $q$  increases. Moreover, when  $q = 10$  the graph bends upwards, which is to be expected from our analytical expansion. In fact, this is so for values of  $q$  larger than 6.6626 approximately, so that the other plots, which correspond to  $q = 5$  and  $q = 3$ , bend downwards. The thick line corresponds to  $\text{Sh}$  versus  $Pe$  for the rigid sphere, indicating that for any value of  $q$  the mass transfer is enhanced by squirming, even though the difference is not significant in this range of  $Pe$ .

**7.1.2 Larger Péclet numbers.** As  $Pe$  increases, the importance of the swimming motions is greater as well, as can be seen from Fig. 6; convergence of the results also depends on  $q$ . In the case of the LPEM, the number  $N$  of terms in (6.1) was varied between 100 and 140, and the outer boundary condition was applied at  $\xi_{\max} = 19$ . As we reach large values of  $Pe$ , small values of  $h$  are required in order to reflect the asymptotic behaviour, otherwise a graph for the numerical results

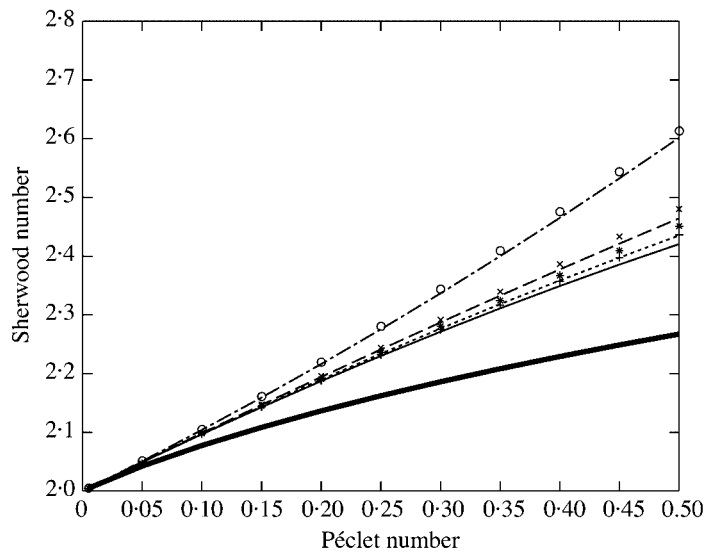


**Fig. 5**  $Sh$  versus  $Pe$  for Péclet numbers up to 0.5. The thick line corresponds to the rigid sphere (numerical result). The curves for  $q = 0.1$  and  $q = 1$  are very close together, so we just show here the results for  $q = 1$  (+: numerical, solid line: analytical), and are the closest to the rigid sphere. The other plots shown correspond to (a)  $q = 3$  (\*: numerical, dotted line: analytical); (b)  $q = 5$  (x: numerical, dashed line: analytical); and  $q = 10$  (o: numerical, dash-dotted line: analytical)

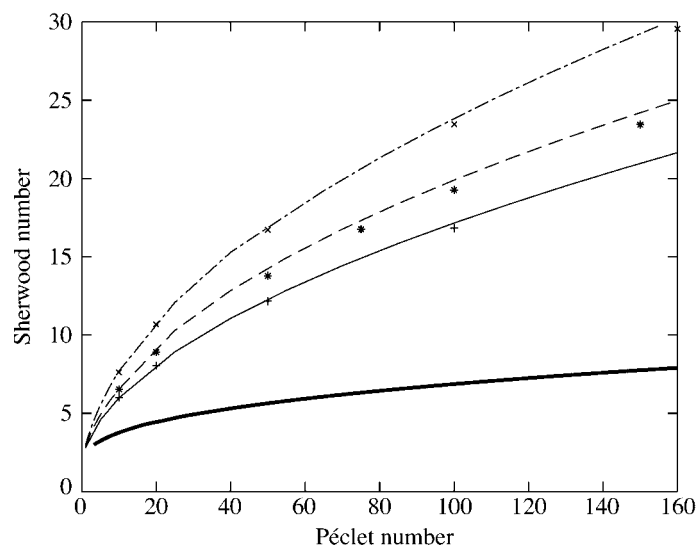


**Fig. 6** Plots for intermediate and large Péclet numbers showing results for the rigid sphere (thick line) and the squirmer when  $q = 0.1$  (solid: LPEM, +: FVM);  $q = 3$  (dashed: LPEM, \*: FVM); and  $q = 5$  (dash-dotted: LPEM, x: FVM). Again, we do not plot the curve corresponding to  $q = 1$  because the results for  $q \leq 1$  are comparable for all  $Pe$

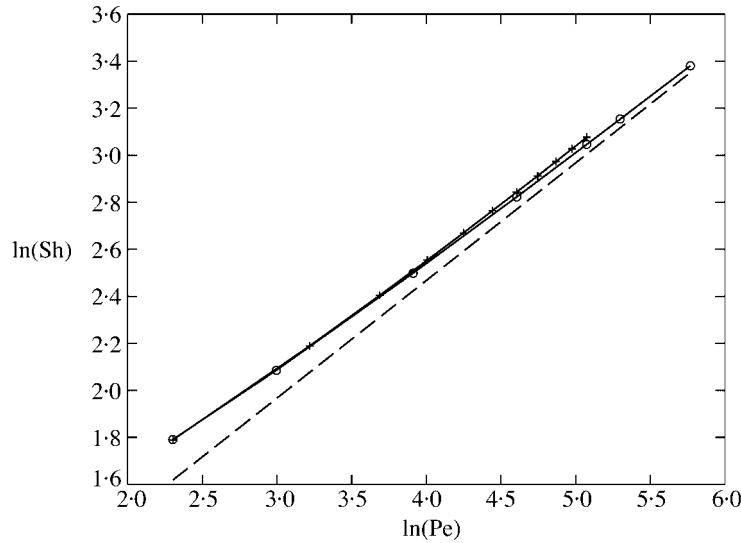


**Fig. 7**  $q = 0.1$ :  $\ln(\text{Sh})$  versus  $\ln(\text{Pe})$  for  $\text{Pe}$  large, with +: LPEM, o: FVM, dashed: boundary-layer theory

such as the ones shown in Figs 7 or 8 would start to bend upwards, instead of slowly converging to the dashed line.

Since the uptake occurs at the surface, we refined the grid in the vicinity of the squirmer by taking  $h = 10^{-2}$  up to a certain  $\xi_0$ , which was modified according to the value of  $q$  being studied. In the case of the FVM, we took  $h = 4 \times 10^{-3}$  everywhere.

For  $q \leq 1$ , we found that both the power  $\frac{1}{2}$  and the proportionality constant  $c$  are well reproduced by the numerical schemes. This can be seen from Fig. 7 and Table 1. The relative error (RE) for the numerical and the theoretical  $c$  is small, although the FVM agrees better.

When  $q > 1$ , we still find the power  $\frac{1}{2}$ , as is shown in Fig. 8 (where  $q = 3$ ), but the discrepancy between theoretical and numerical results increases with  $q$  (see Table 1). However, the two numerical results are comparable, despite the fact that the results of LPEM are restricted to  $\text{Pe} \leq 160$  due to the memory availability of the computer. Therefore the difference with the theory for  $q > 1$  comes from another source.

The concentration contours plotted in Fig. 9 for  $\text{Pe} = 10$  and  $\text{Pe} = 100$ , for  $q = 5$ , indicate that as  $\text{Pe}$  increases the concentration distribution in the recirculation region becomes more uniform and the wake narrower, creating another boundary layer near this part of the surface, so that in the limit of very large Péclet numbers boundary-layer theory might also be applicable at the back of the microorganism, that is, from  $\mu = -1$  to  $\mu = -1/q$ . In this region  $k$ —in equation (5.6)—is  $-\frac{2}{3} + \frac{1}{4}q$  so that  $g$  is bounded at  $\mu = -1$ , and then its contribution to the constant of proportionality is  $\sqrt{\frac{6}{\pi}} \left( -\frac{2}{3} + \frac{q}{4} + \frac{1}{2q} - \frac{1}{12q^3} \right)^{\frac{1}{2}}$ , which means that

$$c_+ = \sqrt{\frac{6}{\pi}} \left\{ \left( \frac{2}{3} + \frac{q}{4} + \frac{1}{2q} - \frac{1}{12q^3} \right)^{\frac{1}{2}} + \left( -\frac{2}{3} + \frac{q}{4} + \frac{1}{2q} - \frac{1}{12q^3} \right)^{\frac{1}{2}} \right\} \quad (7.1)$$

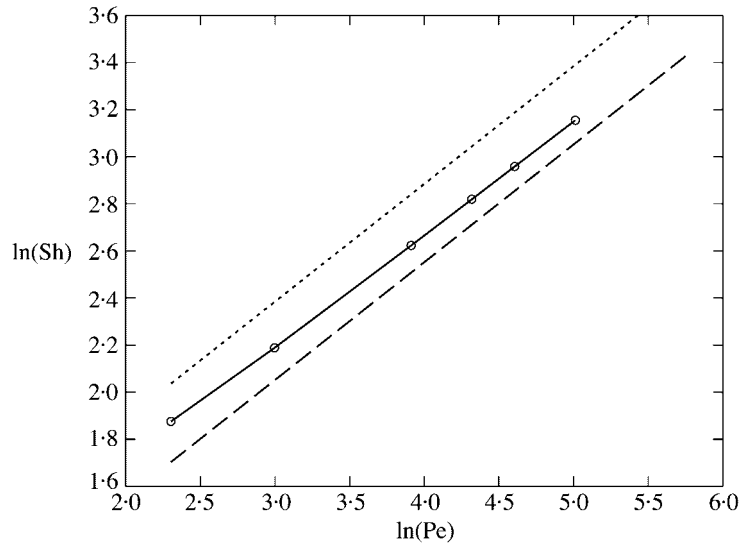


**Fig. 8**  $q = 3$ :  $\ln(\text{Sh})$  versus  $\ln(\text{Pe})$  for  $\text{Pe}$  large, with  $\circ$ : FVM, dashed: boundary-layer theory excluding the recirculation region, dotted: boundary-layer theory applied everywhere

**Table 1** Proportionality constant  $c$ . Comparison of theoretical, LPEM and FVM results

$q$	$c$ from (5.8) and (5.9)	$c$ LPEM	$c$ FVM	RE LPEM	RE FVM	$c_+$ from (7.1)
0.1	1.5957	1.6928	1.6433	6.1%	3.0%	
1	1.5957	1.6928	1.6461	6.1%	32%	
3	1.7366	1.9276	1.8920	11.0%	9.0%	2.424
5	1.9516	2.3787	2.3244	21.9%	19.1%	3.1042

when we apply boundary-layer theory to the whole surface. The constant  $c_+$  obtained following this procedure is shown in Table 1 for  $q = 3$  and  $q = 5$ , and the results with this  $c_+$ , when  $q = 3$ , are plotted in Fig. 8 (dotted line.) We can conclude that, when  $q > 1$ , there is a contribution to the mass transfer from the recirculation region behind the squirmer, but not as much as indicated by equation (7.1). For values of  $\text{Pe}$  between 12.18 and 148.41, the Sherwood number lies between the predictions of the two versions of boundary-layer theory. Rather surprisingly, however, the numerical results become closer to the simple boundary-layer theory (that is, neglecting the recirculating wake region) as  $\text{Pe}$  increases, despite the appearance of a thin rear boundary layer. The resolution of this apparent paradox is presumably that the approximately constant value of  $C$  in the recirculation region is not the value at infinity, zero, but is intermediate between 0 and 1. There appears to be no way of estimating this value at large  $\text{Pe}$ , other than from the numerical results.

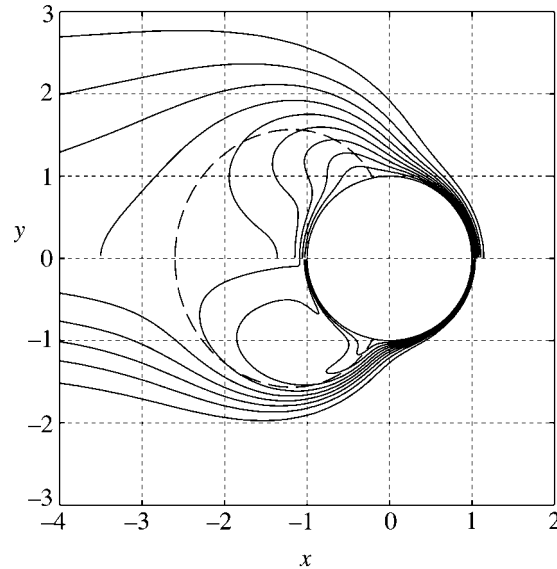


**Fig. 9** Concentration contours ( $q = 5$ ). The upper half corresponds to  $Pe = 10$ , and the lower half to  $Pe = 100$ ; the step between contours is 0.1

Finally, Fig. 6 proves that swimming has a large effect on the nutrient uptake for any value of  $q$ , but such effect is enhanced if  $q \geq 1$ . For instance, when  $Pe = 100$  and  $q = 5$ , the Sherwood number is four times larger in the case of the self-propelled body than for the rigid sphere, and if  $q = 0.1$ , the Sherwood number is only 2.5 times larger.

### 7.2 $q < -1$

We chose  $Pe = 400$  in order to determine the numerical values of  $c_-$  for  $q = -3$  and  $q = -5$ , which we compared with the ones for  $c_+$  shown in Table 1 for  $q = 3$  and  $q = 5$ , respectively. The relative error is smaller than 0.05 per cent in both cases, so we conclude that the symmetry of  $Sh$  with respect to negative and positive values of  $q$  is confirmed. However, Fig. 10 shows how different the concentration distribution is according to whether  $q$  is positive or negative. When  $q$  is negative the wake is much narrower, and the concentration seems to vary smoothly across the recirculation region. The numerical results for intermediate values of  $Pe$  showed that  $Sh$  is symmetric with respect to  $q$  for any value of  $Pe$ , a result which was not expected, for when  $q < -1$  the swimming mechanism seems unphysical.

### 7.3 Alternative boundary condition at large $\xi$

To conclude this section, we now see whether taking the alternative boundary condition given by equation (6.3) at large  $r$  affects the results. We will only show results for the case when  $q = 1$ , since one reaches the same conclusions for any value of  $q$ . Also, for the purposes of this study we

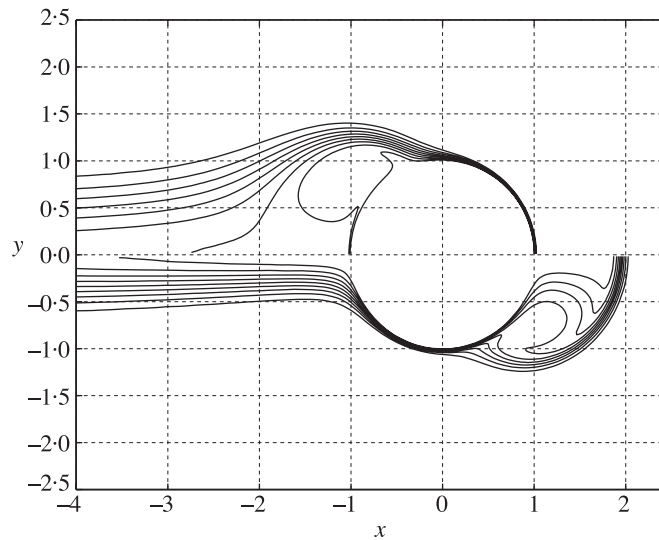


**Fig. 10** Concentration contours ( $Pe = 400$ ). The upper half corresponds to  $q = 3$ , and the lower half to  $q = -3$ ; the step between contours is 0.1

need only to take the value of the outer boundary at  $\xi_{\max} = 3$ —which is the value taken by Dennis *et al.* (11)—since our objective is just to compare the results obtained with the two alternative boundary conditions. Then, if the boundary condition is  $C = 0$ , in the discretization we replace  $C_n(\xi_{\max} + h)$  by 0; if, instead, we exploit the fact that at large  $r$  the concentration distribution behaves as a function proportional to  $\exp(-2\xi)$ , then we take  $C_n(\xi_{\max} + h)$  as  $\exp(-2h) C_n(\xi_{\max})$ .

For intermediate values of the Péclet number, one observes that the RE between the two sets of data is less than  $10^{-3}$  per cent, which is insignificant. For small and for large values of  $Pe$ , shown in Figs 11a and 11b, respectively, the RE becomes larger but remains in a range where we can conclude that the two alternative codes give very similar results, except in the limits of very small or very large  $Pe$ .

However, we also know, from the discussion at the beginning of this section, that when  $Pe$  is small we can take a quite small  $\xi_{\max}$  and apply the boundary condition there since the results vary little if we increase  $\xi_{\max}$  further. This suggests that the type of boundary condition will not affect the result in this range. We can therefore conclude that the type of boundary condition we choose may affect the results but only for values of  $Pe$  which are larger than those considered here.

## 8. Summary and conclusions

In this study we found qualitative and quantitative differences between the steady squirmer and the rigid sphere. We saw that for small  $Pe$  the expansion is regular up to  $O(Pe^2)$ , because there is no external force when the microorganism is self-propelled. We also found that, although the mass transfer is enhanced, the difference is not very significant when diffusion dominates the behaviour. However, as convection becomes more important, the Sherwood number is greater as well, and

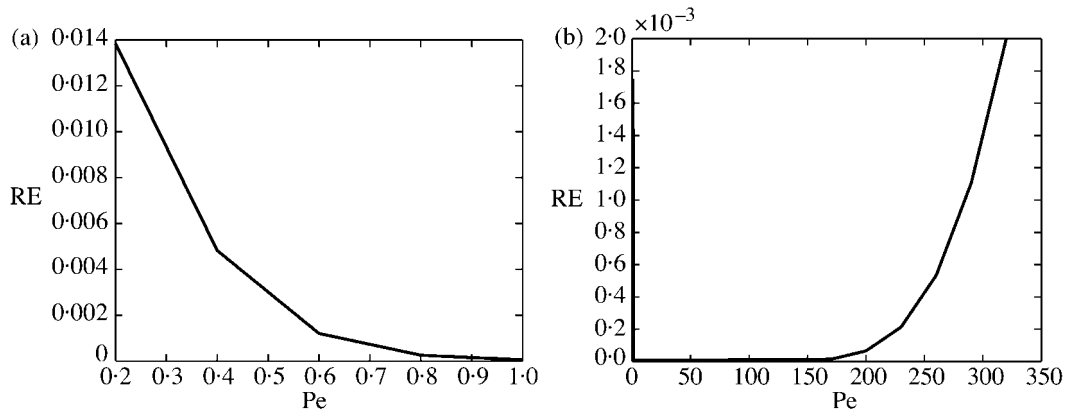


**Fig. 11** This figure shows the relative error (RE) versus Pe, when (a) Pe is small and when (b) Pe is large, between the two alternative boundary conditions at large  $r$

when Pe is large enough Sh becomes asymptotically proportional to  $Pe^{\frac{1}{2}}$ , rather than  $Pe^{\frac{1}{3}}$  as for the rigid sphere. This is as predicted by the boundary-layer theory.

Another parameter affecting the behaviour is  $q$ , which measures the effect of stirring. When  $|q| \leq 1$ , the effect of stirring is almost independent of  $q$ . However, the numerical results show that the mass transfer is enhanced as  $|q|$  increases for values of  $|q|$  larger than 1, and this enhancement is evident for any value of Pe. Also, the Sherwood number is symmetric in  $q$  –  $Sh(q) = Sh(-q)$ , which is to be expected from the theorem by Brenner (10) but is quite surprising since the swimming mode when  $q < -1$  does not seem, intuitively, very effective; however, the concentration distribution of the nutrients is not symmetric in  $q$ .

Finally, when comparing the results for large Péclet numbers, we found that the power of  $\frac{1}{2}$  of the asymptotic behaviour is well reproduced by the numerics. When the stirring parameter  $q$  is less than or equal to one, we obtained good quantitative agreement between numerical and theoretical behaviour. Moreover, for  $q > 1$  plots of concentration contours induced us to think that boundary-layer theory may also be applied in the recirculation region that appears behind the squirmer, because as the Péclet number increases a thin concentration boundary layer appears, outside which the concentration distribution is approximately uniform. Then, the numerical values of the Sherwood number lie between the two theoretical ones, obtained by assuming either one boundary layer, over the front part of the squirmer only, or two, over the rear as well; in both cases the concentration outside the layers is assumed to be the same as at infinity. We conclude that the recirculation region does contribute to mass transfer, but that the uniform concentration within it is not equal to that at infinity.

### Acknowledgements

This work is part of the Ph.D. project of the first author, and is funded by DGAPA, from the National Autonomous University of Mexico. It is also contribution no. 279/40 to the Nutrient Dynamics

Mediated Through Turbulence and Plankton Interactions (NTAP) project, part of the ELOISE project cluster financed by the European Commission. We would like to thank Professor A. Iserles for his advice on the numerical scheme in the LPEM for the rigid sphere.

## References

1. J. R. Moisan and E. E. Hofmann, Modeling nutrient and plankton processes in the California coastal transition zone. 1. A time- and depth-dependent model, *J. Geophys. Res.—Oceans* **C10** **101** (1996) 22647–22676.
2. M. J. Lighthill, On the squirming motion of nearly spherical deformable bodies through liquids at very small Reynolds numbers, *Comm. Pure Appl. Math.* **5** (1952) 109–118.
3. J. R. Blake, A spherical envelope approach to ciliary propulsion, *J. Fluid Mech.* **46** (1971) 199–208.
4. H. A. Stone and A. D. T. Samuel, Propulsion of microorganisms by surface distortions, *Phys. Rev. Lett.* **77** (1996) 4102–4104.
5. K. M. Ehlers, A. D. T. Samuel, H. C. Berg and R. Montgomery, Do cyanobacteria swim using traveling surface waves? *Proc. Natl Acad. Sci. USA* **93** (1996) 8340–8343.
6. J. M. Skerker and H. C. Berg, Direct observation of extension and retraction of type IV pili, *ibid.* **98** (2001) 6901–6904.
7. A. Acrivos and T. D. Taylor, Heat and mass transfer from single spheres in Stokes flow, *Phys. Fluids* **4** (1962) 387–394.
8. S. Childress, *Mechanics of Swimming and Flying*, 1st edition (Cambridge University Press, Cambridge 1981).
9. L. G. Leal, *Laminar Flow and Convective Transport Processes: Scaling Principles and Asymptotic Analysis* (Butterworth–Heinemann, Stoneham 1992).
10. H. Brenner, On the invariance of the heat-transfer coefficient to flow reversal in Stokes and potential streaming flows past particles of arbitrary shape, *J. Math. Phys. Sci.* **1** (1967) 173–179.
11. S. C. R. Dennis, J. D. A. Walker and J. D. Hudson, Heat transfer from a sphere at low Reynolds numbers, *J. Fluid Mech.* **60** (1973) 273–283.
12. A. Iserles and S. P. Nørsett, *Order Stars*, 1st edition (Chapman and Hall, London 1991).
13. M. Abramowitz and I. A. Stegun, *Handbook of Mathematical Functions*, 10th edition (Dover, New York 1972).
14. G. K. Batchelor, Mass transfer from small particles suspended in turbulent fluid, *J. Fluid Mech.* **98** (1980) 609–623.

## APPENDIX A

### *Alternative boundary condition on the surface*

#### A.1 *Small Pe*

One may ask whether a constant concentration distribution is a realistic boundary condition for living organisms. In this Appendix we will see how the results are affected by this simplification. To do so, we suppose that the nutrient is consumed uniformly within the sphere, which requires that we determine the nutrient concentration  $C_{\text{cell}}^*$  inside the sphere; the concentration at the sphere surface is unknown in advance,

and might not be uniform around the surface. We therefore take  $C_{\text{cell}}^*$  to be the solution of the equation

$$\frac{\partial C_{\text{cell}}^*}{\partial t^*} = D_{\text{cell}} \nabla^{*2} C_{\text{cell}}^* - k^2 C_{\text{cell}}^*,$$

where  $D_{\text{cell}}$  is the internal diffusivity, assumed uniform. The first term on the right-hand side describes diffusion, whereas the second corresponds to the consumption of nutrients. If we consider, again,  $r = r^*/a$  to be the non-dimensional distance to the centre of the spherical squirmer, but now  $C = C^*/C_{\infty}^*$  as the non-dimensional concentration, then the steady version of the equation above can be rewritten as

$$\nabla^2 C_{\text{cell}} - \kappa^2 C_{\text{cell}} = 0, \quad (\text{A.1})$$

where  $\kappa = ak/\sqrt{D_{\text{cell}}}$ .

At the surface of the squirmer the transport of nutrients across the membrane is dominated by diffusion. The rate at which the nutrient is flowing to and from the cell is determined by a resistance of the membrane to the passage of nutrients, and at equilibrium the diffusive fluxes from the fluid and into the cell are equal. Therefore, the two boundary conditions we need at  $r = 1$  are

$$D \frac{\partial C_{\text{in}}}{\partial r} = D_{\text{cell}} \frac{\partial C_{\text{cell}}}{\partial r}$$

and

$$\beta [C_{\text{in}} - C_{\text{cell}}] = D_{\text{cell}} \frac{\partial C_{\text{cell}}}{\partial r},$$

where  $C_{\text{in}}$  is the solution of the mass concentration equation outside the cell, but close to the surface, and  $\beta$  is the permeability of the cell membrane. We set  $\beta' = \beta/D$  and  $D' = D_{\text{cell}}/D$ , so the equations above reduce to

$$\frac{\partial C_{\text{in}}}{\partial r} = D' \frac{\partial C_{\text{cell}}}{\partial r} = \beta' (C_{\text{in}} - C_{\text{cell}}). \quad (\text{A.2})$$

Now, we know that  $C_{\text{in}}$  is the regular solution of the mass transfer equation and is of the form

$$C_{\text{in}} = \sum_{n=0}^{\infty} f_n(\epsilon) (C_{\text{in}})_n(r, \mu).$$

Then, in order for  $C_{\text{cell}}$  to satisfy the boundary conditions (A.2) at the surface, it needs to be of the same form, that is,

$$C_{\text{cell}} = \sum_{n=0}^{\infty} f_n(\epsilon) (C_{\text{cell}})_n(r, \mu),$$

and each of the functions  $(C_{\text{cell}})_n$  is the solution of an equation of the type (A.1), because that equation is independent of the Péclet number.

If we set  $(C_{\text{cell}})_n = \sum_{m=0}^{\infty} R_m(r) P_m(\cos \theta)$  and introduce this expansion into equation (A.1), then the radial functions  $R_m$  are solutions of the modified spherical Bessel equation (13), of which two particular solutions are the modified Bessel functions of the first kind,  $\sqrt{\frac{\pi}{2\kappa r}} I_{m+\frac{1}{2}}(\kappa r)$ , and of the third kind,  $\sqrt{\frac{\pi}{2\kappa r}} K_{m+\frac{1}{2}}(\kappa r)$ . Since the functions  $K_{m+\frac{1}{2}}$  diverge at the origin, the functions  $(C_{\text{cell}})_n$  are all given by

$$(C_{\text{cell}})_n = \sum_{m=0}^{\infty} E_m \sqrt{\frac{\pi}{2\kappa r}} I_{m+\frac{1}{2}}(\kappa r) P_m(\cos \theta).$$

In the fluid surrounding the cell, we still have the same steady advection–diffusion equation except that now  $(C_{\text{in}})_0$ , the zero Pe limit, is no longer a constant on the surface. We still assume that the ambient concentration is constant, which means that  $(C_{\text{in}})_0 \rightarrow 1$  as  $r \rightarrow \infty$ . Moreover,  $(C_{\text{in}})_0$  corresponds to the solution near the surface of the organism which is not affected by advection (because it is independent of the Péclet number). Therefore, it cannot have any angular dependence. Since  $(C_{\text{in}})_0$  solves Laplace’s equation, the above boundary conditions lead us to conclude that

$$(C_{\text{in}})_0 = 1 + \frac{A}{r}, \tag{A.3}$$

where  $A$  is constant.

Now, because of the conditions (A.2), it follows that  $(C_{\text{cell}})_0$  is independent of the angular direction as well, and it can then be written as

$$(C_{\text{cell}})_0 = E_0 \frac{\sinh(\kappa r)}{\kappa r}, \tag{A.4}$$

with  $E_0$  an arbitrary constant (13). The constants  $A$ , in equation (A.3), and  $E_0$ , in equation (A.4), will be determined using the boundary conditions (A.2), which can be written as

$$A + D' [\cosh(\kappa) - \sinh(\kappa)/\kappa] E_0 = 0$$

and

$$-\kappa (1 + \beta') A + \beta' \sinh(\kappa) E_0 = \kappa \beta',$$

when we use expressions (A.3) and (A.4), together with their derivatives. Then, from the above we can deduce the explicit values of  $E_0$  and  $A$  and introduce them into equations (A.4) and (A.3), so that

$$(C_{\text{cell}})_0 = \frac{\kappa \lambda}{\kappa \cosh(\kappa) - \sinh(\kappa)} \frac{\sinh(\kappa r)}{\kappa r} \tag{A.5}$$

and

$$(C_{\text{in}})_0 = -\frac{\lambda}{r} + 1, \tag{A.6}$$

respectively, where

$$\lambda = \frac{\beta' D' [\kappa \cosh(\kappa) - \sinh(\kappa)]}{(1 + \beta') D' \kappa \cosh(\kappa) + (\beta' - D' - \beta' D') \sinh(\kappa)}. \tag{A.7}$$

We note that  $\lambda$  is positive for all (positive) values of the constants  $\kappa$ ,  $\beta'$ ,  $D'$ , as it must be for the concentration at the sphere surface to be less than it is far away. From the small Pe expansion of section 4 above, the leading term corresponds to taking  $\lambda = 1 - C_0^*/C_\infty^*$  in (A.6).

We now need a new definition of the Sherwood number. In analogy to (14), the instantaneous rate of mass transfer into the cell is given by

$$Q = D \int_A \mathbf{n} \cdot \nabla^* C^* dA = 2\pi a^2 D \int_{-1}^1 \left( \frac{\partial C^*}{\partial r^*} \right)_{r^*=a} d\mu = 2\pi a D C_\infty^* \int_{-1}^1 \left( \frac{\partial C}{\partial r} \right)_{r=1} d\mu,$$

with  $\mu = \cos \theta$ , since the cell is a sphere of radius  $a$ . If  $Q_0$  is the instantaneous rate of mass transfer due to diffusion alone, and if we define the Sherwood number as  $\text{Sh} = Q/Q_0$ , so that  $\text{Sh}_0 = 1$ , then from the above we deduce that

$$\text{Sh} = \frac{1}{2\lambda} \int_{-1}^1 \left( \frac{\partial C_{\text{in}}}{\partial r} \right)_{r=1} d\mu. \tag{A.8}$$

Let us consider the new variable  $C^n = C - 1$ . Then,

$$(C_{\text{in}}^n)_0 = -\frac{\lambda}{r} \quad (\text{A.9})$$

and

$$(C_{\text{out}}^n)_0 = -\frac{\lambda}{\rho} \exp\left[\frac{\rho}{2}(-\mu - 1)\right]. \quad (\text{A.10})$$

We now want to find the first-order term  $(C_{\text{in}}^n)_1$ , which is a solution of the equation

$$\nabla^2 (C_{\text{in}}^n)_1 = -\lambda \left( \frac{1}{r^2} - \frac{1}{r^5} \right) \mu + \frac{3\lambda}{2B_1} \sum_{n=2}^{\infty} \left( \frac{1}{r^{n+4}} - \frac{1}{r^{n+2}} \right) B_n P_n(\mu).$$

It is straightforward to deduce that the general solution of the equation above is

$$\begin{aligned} (C_{\text{in}}^n)_1 &= \frac{\lambda\mu}{2} \left( 1 + \frac{1}{2r^3} \right) + \frac{3\lambda}{2B_1} \sum_{n=2}^{\infty} \left[ \frac{1}{2(n+1)r^{n+2}} + \frac{1}{2nr^n} \right] B_n P_n(\mu) \\ &+ \sum_{n=0}^{\infty} \left[ \hat{D}_n r^n + \hat{E}_n r^{-(n+1)} \right] P_n(\mu). \end{aligned} \quad (\text{A.11})$$

We next proceed to match  $(C_{\text{in}}^n)_1$  with  $(C_{\text{out}}^n)_0$ . The matching requirement is that

$$(C_{\text{in}}^n)_1 \approx \frac{\lambda\mu}{2} + \hat{D}_0 + \hat{D}_1 r \mu + \sum_{n=2}^{\infty} \hat{D}_n r^n P_n(\mu).$$

Then, we deduce that  $\hat{D}_{n \geq 1} = 0$ , and  $\hat{D}_0 = \frac{1}{2}\lambda$  as opposed to  $-\frac{1}{2}$  when assuming that the concentration is constant at the boundary. With our new boundary conditions,  $(C_{\text{in}}^n)_1$  and  $(C_{\text{cell}}^n)_1$  satisfy equations of the form (A.2) when  $r = 1$ , that is,

$$-\hat{E}_0 P_0(\mu) + \dots = D' E_0 (\cosh(\kappa) - \sinh(\kappa)/\kappa) P_0(\mu) + \dots \quad (\text{A.12})$$

and

$$-\hat{E}_0 P_0(\mu) + \dots = \beta' \left( \frac{1}{2}\lambda + \hat{E}_0 - E_0 \sinh(\kappa)/\kappa \right) P_0(\mu) + \dots, \quad (\text{A.13})$$

and so the two constants  $E_0$  and  $\hat{E}_0$  are linked by the conditions at the cell's surface. Solving the system of equations (A.12) and (A.13), we deduce that  $\hat{E}_0 = -\frac{1}{2}\lambda^2$ , and since

$$\text{Sh}_1 = -\frac{1}{2\lambda} \int_{-1}^1 \left( \frac{\partial (C_{\text{in}}^n)_1}{\partial r} \right)_{r=1} d\mu = \frac{\hat{E}_0}{\lambda} = -\frac{\lambda}{2},$$

we conclude that the Sherwood number term of  $O(\epsilon)$  is reduced with these new boundary conditions, because it is equal to  $-\frac{1}{2}\lambda$ , which is negative, and not  $\frac{1}{2}$  as in the case with constant nutrient concentration at the surface.

Further modifications to the results would be observed if we continued the analysis to higher orders of the Péclet number expansion, but the study carried out so far has already demonstrated that the results are affected when we consider other types of boundary conditions which may be closer to reality. However, in the example considered here, the form of the expansion of Sh remains the same, and the variations are seen in the coefficients of the expansion, which now depend on the membrane permeability  $\beta'$  and the nutrient consumption factor  $\kappa$ .

A.2 Large Pe

When the Péclet number is large, certain similarities with the case studied previously arise naturally. For instance, boundary-layer theory should still be applicable for the concentration distribution outside the sphere, but now it is possible that no similarity solution is available. In that case the Sherwood number would not be proportional to the square root of the Péclet number, but to another power of Pe, or a more intricate function of Pe instead. To check this, we need to explore in more detail the implication of having a variable concentration at the surface of the microorganism.

In order for convection and diffusion to be of similar order in the boundary layer, the change of variable  $Y = \text{Pe}^{\frac{1}{2}}(r - 1)$  remains valid, and equation (5.2) still holds for  $C_{\text{ext}}$ , the nutrient concentration distribution in the vicinity of the membrane and external to the cell. The local variable  $Y$  represents a Cartesian coordinate perpendicular to the microorganism's surface. We consider again the change of variable  $\eta = Y/g(\mu)$ , by analogy with the analysis in section 5, but keep in mind that now  $\eta$  does not correspond to a similarity variable, since  $C_{\text{ext}}$  might depend not only on  $\eta$  but on  $\mu$  as well. Then,

$$\frac{\partial^2 C_{\text{ext}}}{\partial \eta^2} + 2f(\mu)\eta \frac{\partial C_{\text{ext}}}{\partial \eta} = 0,$$

with  $f(\mu) = \frac{3}{2}g^2[\mu + qP_2(\mu)] - \frac{3}{8}(1 - \mu^2)(1 + q\mu)(g^2)'$ . Remember that the non-dimensional concentration is defined as  $C_{\text{ext}} = C_{\text{ext}}^*/C_{\text{ext}}^\infty$ , so that  $C_{\text{ext}} \rightarrow 1$  when  $r$ , or  $\eta$ , tends to infinity. The solution of the equation above, together with the boundary condition we have just discussed, may be written as

$$C_{\text{ext}} = 1 + A \int_{\eta}^{\infty} \exp[-f(\mu)t^2] dt,$$

which leads to  $C_{\text{ext}}(\eta = 0) = 1 + \sqrt{\frac{\pi}{2f(\mu)}}A$ , and  $\frac{\partial C_{\text{ext}}}{\partial \eta}(\eta = 0) = -A$ , on the surface of the cell.

The inner solution is still dependent on  $r$  and  $\mu$  but, if  $A$  should turn out to be very small as  $\text{Pe} \rightarrow \infty$ , the leading-order term of the solution of equation (A.1) will again be spherically symmetric and given by (A.4). Then, the boundary conditions take the form

$$-vA = D'E_0 \left[ \cosh(\kappa) - \frac{\sinh(\kappa)}{\kappa} \right] = \beta' \left[ 1 + \sqrt{\frac{\pi}{2f(\mu)}}A - E_0 \frac{\sinh(\kappa)}{\kappa} \right],$$

with  $v = \text{Pe}^{\frac{1}{2}}/g(\mu) \gg 1$ . Now, assuming that  $\beta'$ ,  $D'$  and  $\kappa$  are all  $O(1)$ , the first equality implies that  $E_0 \gg A$ , and since

$$E_0 \left\{ D' \cosh(\kappa) \left( 1 + \frac{\beta'}{v} \sqrt{\frac{\pi}{2f(\mu)}} \right) + \frac{\sinh(\kappa)}{\kappa} \left[ \beta' - D' \left( 1 + \frac{\beta'}{v} \sqrt{\frac{\pi}{2f(\mu)}} \right) \right] \right\} = \beta',$$

we deduce that  $E_0$  is of order 1 as well, and that  $E_0 \{ D' \cosh(\kappa) + (\beta' - D') \sinh(\kappa)/\kappa \} \approx \beta'$ . Therefore,  $A = O(\text{Pe}^{-\frac{1}{2}})$  is very small and we may assume that  $1 - C_{\text{ext}} = O(\text{Pe}^{-\frac{1}{2}}) \ll 1$ , so that  $[\partial C_{\text{ext}}/\partial \eta]_{\eta=0} = O(\text{Pe}^{-\frac{1}{2}})$  and  $[\partial C_{\text{ext}}/\partial r]_{r=1} = O(1)$ . Hence the Sherwood number, as defined in (A.8), is given for  $\text{Pe} \gg 1$  as

$$\text{Sh} \approx \frac{\beta'}{\lambda}, \tag{A.14}$$

where  $\lambda$  is given by (A.7). This is greater than 1 but certainly  $O(1)$ , so the reduction in Sh seen from the small Pe expansion is even more marked at large Pe. It is interesting to note that the quantity defined by (A.14) is independent of the nature or speed of the sphere's squirming, at leading order. This is quite unlike the case with a constant concentration at the boundary. However, the squirming is essential, because it is that which

causes the concentration boundary layer on the sphere's surface to be so thin that the internal concentration is spherically symmetric, and the external concentration to be only infinitesimally reduced below its value at infinity. Further investigation of this problem, at intermediate values of the Péclet number, would be of interest.

## APPENDIX B

Functions  $R_1, \dots, R_4$  in  $(C_{in})_2$

The functions  $R_1, \dots, R_4$  in the second-order term of the small Péclet number asymptotic expansion for the concentration field are of the form

$$\begin{aligned} R_1(r) &= -\frac{1}{4} - \left(\frac{3q}{40}\right) \frac{1}{r} + \left(\frac{11q}{40} - \frac{1}{8}\right) \frac{1}{r^3} \\ &\quad + \left(\frac{3q}{400}\right) \frac{1}{r^4} - \left(\frac{11q}{80}\right) \frac{1}{r^5} + \left(\frac{23q}{560}\right) \frac{1}{r^6}, \\ R_2(r) &= \frac{r}{12} - \frac{1}{4r} + \left(\frac{5}{24} - \frac{3q}{16}\right) \frac{1}{r^2} + \left(\frac{9q^2}{140}\right) \frac{\ln(r)}{r^3} \\ &\quad - \left(\frac{1}{8} + \frac{q}{8} - \frac{15q^2}{112}\right) \frac{1}{r^4} + \left(\frac{5}{168} + \frac{3q^2}{784}\right) \frac{1}{r^5} \\ &\quad - \left(\frac{5q^2}{112}\right) \frac{1}{r^6} + \left(\frac{5q^2}{336}\right) \frac{1}{r^7}, \\ R_3(r) &= \left(\frac{3q}{40}\right) \frac{1}{r} - \left(\frac{3q}{16}\right) \frac{1}{r^2} - \left(\frac{q}{40}\right) \frac{1}{r^3} \\ &\quad + \left(\frac{9q}{140}\right) \frac{\ln(r)}{r^4} - \left(\frac{33q}{160}\right) \frac{1}{r^5} + \left(\frac{13q}{240}\right) \frac{1}{r^6}, \\ R_4(r) &= \left(\frac{81q^2}{1960}\right) \frac{1}{r^3} - \left(\frac{81q^2}{448}\right) \frac{1}{r^4} \\ &\quad + \left(\frac{9q^2}{140}\right) \frac{\ln(r)}{r^5} - \left(\frac{9q^2}{112}\right) \frac{1}{r^6} + \left(\frac{9q^2}{385}\right) \frac{1}{r^7}. \end{aligned}$$

## APPENDIX C

Values of the constants  $\alpha_i$  and  $\beta_{i,j}$

In this Appendix we give the values of the constants  $\alpha_i$  and  $\beta_{i,j}$  which appear in section 6.

For  $i = 1$ , we have that

$$\alpha_1(n, n+1) = \frac{n+1}{2n+3},$$

$$\alpha_1(n, n-1) = \frac{n}{2n-1},$$

and for  $i = 2$ ,

$$\alpha_2(n, n-2) = \frac{3}{2} \frac{n(n-1)}{(2n-1)(2n-3)},$$

$$\alpha_2(n, n) = \frac{n(n+1)}{(2n-1)(2n+3)},$$

$$\alpha_2(n, n+2) = \frac{3}{2} \frac{(n+1)(n+2)}{(2n+3)(2n+5)}.$$

The values for  $\beta_{0,2}$  are

$$\beta_{0,2}(n, n+1) = \frac{3}{2} \frac{(n+1)(n+2)}{2n+3},$$

$$\beta_{0,2}(n, n-1) = -\frac{3}{2} \frac{n(n-1)}{2n-1},$$

whereas for  $\beta_{1,3}$  we get

$$\beta_{1,3}(n, n-2) = -\frac{5}{2} \frac{n(n-1)(n-2)}{(2n-1)(2n-3)},$$

$$\beta_{1,3}(n, n) = \frac{5}{2} \frac{n(n+1)}{(2n-1)(2n+3)},$$

$$\beta_{1,3}(n, n+2) = \frac{5}{2} \frac{(n+1)(n+2)(n+3)}{(2n+5)(2n+3)}.$$